

Nanofiltration of multi-ionic solutions: prediction of ions transport using the SEDE model

A.I. Cavaco Morão¹, A. Szymczyk^{2,3}, P. Fievet⁴ and A.M. Brites Alves^{1*}

¹*Instituto Superior Técnico, Department of Chemical and Biological Engineering,
Av. Rovisco Pais 1, 1049-001 Lisboa, Portugal*

²*Université Européenne de Bretagne, France*

³*Université de Rennes 1, CNRS, Laboratoire des Sciences Chimiques de Rennes,
UMR 6226 CNRS/UR1/ENSCR, Chimie et Ingénierie des Procédés, 263 Av. du Général Leclerc,
Bât. 10 A, CS 74205, F-35042 Rennes, France*

⁴*Institut UTINAM, UMR CNRS 6213, Université de Franche-Comté, 16 route de Gray,
Besançon Cedex 25030, France*

(Received September 24, 2009, Accepted February 22, 2010)

Abstract. This work focuses on the application of nanofiltration (NF) to the concentration of a pharmaceutical product, Clavulanate (CA^-), from clarified fermentation broths, which show a complex composition with six main identified ions (K^+ , Cl^- , NH_4^+ , H_2PO_4^- , SO_4^{2-} and CA^-), glucose and glycerol. The solutes transport through the NF membrane pores was investigated using the SEDE (Steric, Electric and Dielectric Exclusion) model. This model was applied to predict the rejection rates of the initial feed solution and the final concentrated solution (10-fold concentrated solution). The best results were achieved with a single fitted parameter, ε_p (the dielectric constant of the solution inside pores) and considering that the membrane selectivity is governed by steric, electric (Donnan) and Born dielectric exclusion mechanisms. While the predicted intrinsic rejections of solutions comprising up to six ions and uncharged solutes were in good agreement with the experimental values, the deviations were much larger for the 10-fold concentrated solution.

Keywords: nanofiltration; multi-ionic solutions; transport model; membrane charge; concentration polarization.

1. Introduction

In a recent review by Van der Bruggen, *et al.* (2008) the need of tools aiming for the modelling of the performance of nanofiltration (NF), comprising both flux and rejection prediction, was identified as drawback contributing to slow down large-scale applications of NF. This work is a contribution to the knowledge of the mass transfer and separation mechanisms governing the NF of multi-component solutions, necessary to develop a suitable model. The application of NF to the isolation of a pharmaceutical product, clavulanic acid, produced industrially by fermentation was studied here. NF is applied to the aqueous solution obtained by the solid-liquid separation performed upon the broth, coming from the fermentation step. This complex aqueous solution contains six main ions (CA^- , K^+ , Cl^- , H_2PO_4^- , NH_4^+ and SO_4^{2-}) and also uncharged solutes, the most representative being glucose and glycerol.

* Corresponding author, Ph.D. E-mail: ana.b.alves@ist.utl.pt

Throughout this work a multi-scale approach to NF of multi-component solutions was pursued: the selectivity of a membrane is determined at the entrance and inside the nanopores even though the concentration of solute that reaches the membrane surface results from the hydrodynamics in the feed solution/membrane vicinity. As the membrane separation properties are known to depend on the interactions between the solution and the membrane surface, the properties of the membrane surface contacting the solution must be assessed. The overall performance of the membrane results from these phenomena, which were addressed and integrated in this work.

The strategy followed is based on the state-of-the-art mechanisms governing the separation of single salt (and uncharged solutes) solutions. The concentration of solutes at the membrane surface was calculated using the appropriate mass transfer correlation for the plate-and-frame membrane module used and a simple model to predict concentration polarization in multi-ionic solutions (Geraldes and Afonso 2007). The solutes transport through the NF membrane pores was investigated using the SEDE (Steric, Electric and Dielectric Exclusion) model developed by (Szymczyk and Fievet 2005). The innovation of the current work relies on the extension of those mechanisms as well as the existing model to the case of concentrated multi-component solutions (mixed charged and uncharged solutes). In a previous publication the mechanisms governing the separation of five or six ions solutions were investigated (Cavaco Morão, *et al.* 2008, 2008a). In the current work the application of the SEDE model is further extended to investigate the impact of the uncharged solutes (glucose and glycerol) on the overall rejections of the six ions solutions. Furthermore, this model was applied to predict the rejection rates of the initial feed solution and a final 10-fold concentrated solution.

The best match between the model predictions and the experimental results were achieved with a single fitted parameter (ε_p , the dielectric constant of the solution inside pores) and considering that the membrane selectivity is governed by steric, electric (Donnan) and Born dielectric exclusion mechanisms. The membrane volume charge density was assessed from tangential streaming potential measurements for each system membrane/electrolyte solution investigated.

2. NF model

For the modelling of the mass transport in NF four main contributions have been considered each one of these playing a definitive role in the whole transport process. Being so we considered : 1) concentration polarization at the feed side - determines the concentration at the interface feed solution/membrane, outside the membrane, 2) equilibrium partitioning of species at the feed/membrane interface- rules the concentration at the feed/membrane interface, inside the membrane, 3) solute transport through the pores by a combination of convection, diffusion and electromigration (for charged solutes only), and 4) equilibrium partitioning of species at the membrane/permeate interface (the same as 2) but now for the permeate side. The approach of Geraldes and Afonso (2007) is used to describe 1) and the SEDE model (Szymczyk and Fievet 2005) was applied to describe the steps 2) to 4). It was assumed that the contribution of the support layer to the solutes separation is negligible. These contributions are presented in Fig. 1.

The effect of concentration polarization was considered and the value of the concentration at the membrane wall of each ion in solution ($C_{i,m}$) was calculated using the simplified approach proposed by Geraldes and Afonso (2007), which applies to dilute multi-ionic solutions. The equations used for concentration polarization calculations are summarized in Table 1. This method was used with the film theory and the mass-transfer correlation derived by Computational Fluid Dynamics ($64 < \text{Re} < 570$

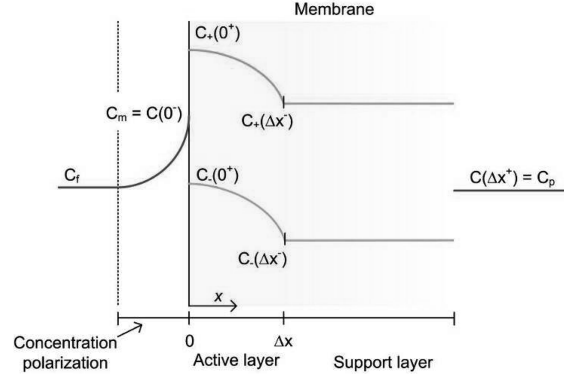


Fig. 1 Representation of 1:1 salt concentration gradients adjacent to the membrane due to concentration polarization, partition at the pores entrance, concentration gradients inside the membrane pores and partition at the pores outlet. Subscripts: -anion and +cation

and $450 < Sc_i < 8900$) for the plate-and frame membrane module used in this work (Cavaco Morão, *et al.* 2008b):

$$Sh_i = 0.142 Re^{0.46} Sc_i^{0.37} \quad (1)$$

The concentrations of uncharged solutes at the membrane wall were calculated, as well, using the film theory and the mass transfer correlation above, Eq. (1).

The transport of solutes within the membranes pores and at both the interfaces feed/membrane and membrane/permeate is described by the SEDE model which is extensively described in the literature (Szymczyk and Fievet 2005, Szymczyk, *et al.* 2006, 2007, 2007b). This homogeneous 1D model is based in simplifying assumptions such as: i) the membrane is a collection of straight capillary pores either with cylindrical or slit-like geometry and ii) the radial variations of electrical potential and ion concentration inside pores can be neglected. The transport of solutes within the membrane pores is accounted for using the extended Nernst - Planck equations (ENP) and interfacial phenomena are described as being due to steric hindrance, Donnan exclusion and dielectric exclusion. A summary of the transport equations within the membrane using the SEDE

Table 1 Equations for calculation of concentration polarization of multi-ionic solutions (all symbols are defined in nomenclature section)

$$J_v C_{i,m} R_i = k_i \Xi_i (C_{i,m} - C_{i,f}) + z_i C_{i,m} D_i \frac{F}{RT} \xi \quad (2)$$

with:
$$\Xi_i = \phi_i + \frac{\phi_i}{\exp(\phi_i) - 1} \quad (\text{film theory}) \quad \text{and} \quad \phi_i = J_v / k_i. \quad (3)$$

Electroneutrality at the feed solution/membrane interface:

$$\sum_{i=1}^n z_i C_{i,m} = 0 \quad (4)$$

model is given in Table 2.

As it is well known, both steric restrictions and particle-wall hydrodynamic interactions reduce the diffusivities of solutes inside the membrane pores. These reductions are accounted through the introduction of simplified equations in the transport models which contain convection and diffusion

Table 2 Transport equations within the membrane used in the SEDE model (all symbols are defined in nomenclature)

Zero electric current condition (steady state):

$$F \sum_{i=1}^n z_i j_i = 0 \quad (5)$$

Transport equations:

$$j_i = -K_{i,d} D_i \frac{dC_i}{dx} - \frac{z_i C_i K_{i,d} D_i F d\psi}{RT dx} + K_{i,c} C_i V = \frac{J_v C_i (\Delta x^+)}{A_k} \quad (6)$$

Concentration gradients inside pores:

$$\frac{dC_i}{dx} = \frac{J_v}{K_{i,d} D_i A_k} (K_{i,c} C_i - C_{i,p}) - \frac{z_i C_i F d\psi}{RT dx} \quad (7)$$

Electrical potential gradient inside pores:

$$\frac{d\psi}{dx} = \frac{\sum_{i=1}^n \frac{z_i J_v}{K_{i,d} D_i A_k} [K_{i,c} C_i - C_i (\Delta x^+)]}{\frac{F}{RT} \sum_{i=1}^n z_i^2 C_i} \quad (8)$$

Table 3 Hindrance factors for diffusion and convection in cylindrical and slit-like pores, $0 \leq \lambda_i < 1$

Cylindrical pores	Slit pores
Diffusion:	Diffusion:
$K_{i,d} = \frac{H(\lambda_i)}{\Phi_i}$	$K_{i,d} = \frac{H(\lambda_i)}{\Phi_i}$
$H(\lambda_i) = 1 + \frac{9}{8} \lambda_i \ln \lambda_i - 1.56034 \lambda_i + 0.528155 \lambda_i^2$ $+ 1.91521 \lambda_i^3 - 2.81903 \lambda_i^4 + 0.270788 \lambda_i^5$ $+ 1.10115 \lambda_i^6 - 0.435933 \lambda_i^7$	$H(\lambda_i) = 1 + \frac{9}{16} \lambda_i \ln \lambda_i - 1.19358 \lambda_i$ $+ 0.4285 \lambda_i^3 - 0.3192 \lambda_i^4 + 0.08428 \lambda_i^5$
Convection:	Convection:
$K_{i,c} = \left(\frac{1 + 3.867 \lambda_i - 1.907 \lambda_i^2 - 0.834 \lambda_i^3}{1 + 1.867 \lambda_i - 0.741 \lambda_i^2} \right)$	$K_{i,c} = \frac{W(\lambda_i)}{\Phi_i}$
	$W(\lambda_i) = 1 - 3.02 \lambda_i^2 + 5.776 \lambda_i^3 - 12.3675 \lambda_i^4$ $+ 18.9775 \lambda_i^5 - 15.2185 \lambda_i^6 + 4.8525 \lambda_i^7$

hindrance for uncharged spheres in pores (Deen 1987). This theory of hindered transport in pores was reviewed and enhanced recently by Dechadilok and Deen (2006). These new equations, shown in Table 3, were applied in this work.

For dielectric exclusion two main contributions are considered in the SEDE model: i) a modified

Table 4 Partitioning equations used in the SEDE model (all symbols are defined in nomenclature)

Partitioning equations at the membrane/solution interfaces:	
$\frac{C_i(0^+)}{C_i(0^-)}$	$= \Phi_i \exp\left(-\frac{z_i e \Delta \Psi_{(0^+ 0^-)}}{kT}\right) \exp\left(-\frac{\Delta W_{i,(0^+ 0^-)}}{kT}\right) \left(\frac{\gamma_i(0^-)}{\gamma_i(0^+)}\right)$ (9)
$\frac{C_i(\Delta x^-)}{C_i(\Delta x^+)}$	$= \Phi_i \exp\left(-\frac{z_i e \Delta \Psi_{(\Delta x^- \Delta x^+)}}{kT}\right) \exp\left(-\frac{\Delta W_{i,(\Delta x^- \Delta x^+)}}{kT}\right) \left(\frac{\gamma_i(\Delta x^+)}{\gamma_i(\Delta x^-)}\right)$ (10)
Steric exclusion:	
	$\Phi_i(\lambda_i) = (1 - \lambda_i)^2$ (cylindrical pores) (11)
	$\Phi_i(\lambda_i) = (1 - \lambda_i)$ (slit-like pores) (12)
Born dielectric exclusion:	
	$\Delta W_{i,Born} = \frac{(z_i e)^2}{8\pi\epsilon_o r_{i,cav}} \left(\frac{1}{\epsilon_p} - \frac{1}{\epsilon_b}\right)$ (13)
Dielectric exclusion due to image forces:	
Cylindrical pores:	$\Delta W_{i,im(0^+ 0^-)} = kT \frac{2\alpha_i}{\pi} \int_0^\infty \frac{K_0(k')K_1(v) - \tilde{\beta}(k')K_0(k')K_1(v)}{I_1(k')K_0(k') + \tilde{\beta}(k')I_0(v)K_1(v)} dk'$ (14)
Slit like pores:	$\Delta W_{i,im(0^+ 0^-)} = -\alpha_i kT \ln \left[1 - \left(\frac{\epsilon_p - \epsilon_m}{\epsilon_p + \epsilon_m}\right) \exp(-2\mu'_{(0^+ 0^-)}) \right]$ (15)
I_0, I_1, K_0 and K_1 are the modified Bessel functions; k' the wave vector;	
$\alpha_i = \frac{(z_i F)^2}{8\pi\epsilon_o\epsilon_p RT N_A r_p}$; $v = \sqrt{k'^2 + \mu'^2_{(0^+ 0^-)}}$; $\tilde{\beta} = \frac{k'}{\sqrt{k'^2 + \mu'^2_{(0^+ 0^-)}}} \left(\frac{\epsilon_m}{\epsilon_p}\right)$ and	
$\mu'_{(0^+ 0^-)}$	$= \kappa^{-1}(0^-) r_p \sqrt{\frac{z_i^2 C_i(0^-) \Phi_i \exp\left(-\frac{\Delta W_{i,Born} + \Delta W_{i,im(0^+ 0^-)} + z_i \Delta \Psi_{(0^+ 0^-)}}{kT}\right) \gamma_i(0^-)}{\gamma_i(0^+)}$
Electroneutrality conditions:	
$\sum_{i=1}^n z_i C_i(0^-) = 0$; $\sum_{i=1}^n z_i C_i(\Delta x^+) = 0$; $\sum_{i=1}^n z_i C_i + X = 0$, for $0^+ \leq x \leq \Delta x^-$ (16)	

Born effect which, instead of considering the ionic radius of the species, as stated in the original Born model, uses the radius of the cavity formed by the ion i in the solvent, $r_{i,cav}$ (Rashin and Honig 1985) and ii) the “image forces” effect first studied and set up by Yaroshchuk (2000) and applied to the SEDE model in previous works (Szymczyk and Fievet 2005, Szymczyk, *et al.* 2006, 2007, 2007b, Cavaco Morão, *et al.* 2008). The equations used for the partitioning calculations are summarized in Table 4.

In this work it is assumed that the gradient of activity coefficients inside the membrane can be neglected, which implies that either the concentrations within pore are small or their variations are very small (Shäfer, *et al.* 2005).

There are evidences of water structural changes in confined systems influencing its physical properties, such as viscosity (Bowen and Welfoot 2002). However, as quantitative studies dealing with the increase of water viscosity in pores lack, in this study the bulk water viscosity is used.

Assuming that the dielectric constant of the active layer of polyamide membranes used in this work has the value of $\varepsilon_m=3$ (Bandini and Vezzani 2003, Szymczyk and Fievet 2005, Szymczyk, *et al.* 2006, 2007), the SEDE model contains four other parameters: 1) the membrane average pore radius r_p , 2) the membrane thickness to porosity ratio $\Delta x/A_k$, 3) the membrane volume charge density X and 4) the dielectric constant of the solution-filled pores (ε_p). The pore radius as well as the membrane thickness to porosity ratio was estimated through independent retention experiments of uncharged solutes. The membrane volume charge density X was determined by tangential streaming potential measurements. Therefore, the single fitting parameter of the model is ε_p . The inputs of the SEDE model were the volumetric permeate fluxes, J_v and the concentration at the membrane surface ($C_{i,m}$).

The outputs of the model were the values of $C_{i,p}$ which were then used to calculate the intrinsic rejection rates (*i.e.* predicted intrinsic rejection rates, $R_{i,model}$).

In the case of uncharged solutes solutions, the transport model (Table 2) can be simplified by considering that the transport of uncharged solutes inside the membrane results only from the diffusive and convective fluxes, *i.e.* size exclusion is considered as the only separation mechanism (Bowen and Mukhtar 1996):

$$R_i = 1 - \frac{C_{i,p}}{C_{i,m}} = 1 - \frac{\Phi_i K_{i,c}}{1 - [(1 - \Phi_i K_{i,c})(\exp(-Pe))]} \quad (17)$$

where $K_{i,c}$ and $K_{i,d}$ are the convective and diffusive hindrance factors (*v.d.* Table 3). Peclet permeation number, Pe , is defined as:

$$Pe = \frac{K_{i,c} J_v \Delta x}{K_{i,d} D_i A_k} \quad (18)$$

where J_v is the permeation flux and D_i the diffusivity of the solute i at infinite dilution. $\Phi_i(\lambda_i)$ is the steric term that accounts for the size of the solutes. Assuming that only steric interactions between the solute and the membrane pore are considered and the solute velocity is fully developed inside the pore, $\Phi_i(\lambda_i)$ is calculated through Eq. (10) or Eq. (11).

The rejection rates of the uncharged solutes were determined using Eq. (17) with the convective and diffusive hindrance factors listed in Table 3.

Throughout this study it was necessary to compare the intrinsic rejections rates based on the experimental data with the model predictions ($R_{i,model}$). The quality of the fit was evaluated through

the use of a least-squares objective function, S_y . If there are n solutes and j data points for each solute, S_y is defined as follows:

$$S_y = \sqrt{\frac{\sum_{i=1}^n \sum_{j=1}^j (R_i - R_{i,model})^2}{jn-1}} \quad (19)$$

3. Experimental

3.1. Membranes and chemicals

The membrane used for this study was the thin film composite membrane Desal DK (GE Osmonics). All chemicals except potassium clavulanate were of analytical grade and solutions were prepared with milli-Q quality water. The potassium clavulanate (KCA, MW = 237 g/mol) used for the NF and tangential streaming potential measurements was supplied by CIPAN (lot 315.45 B 008).

3.2. Nanofiltration experiments

All filtration experiments were carried out on a plate-and-frame LabStak M20 unit (Alfa Laval) at $15 \pm 0.5^\circ\text{C}$. The details of the filtration experiments were described elsewhere (Cavaco Morão, *et al.* 2008).

3.3. Characterization of the process streams

The model solutions were prepared at a pH of 5.5 ± 0.2 with salts concentrations of $(\text{NH}_4)_2\text{SO}_4$ (0.5 g/l), KCl (0.21 g/l), KH_2PO_4 (0.05 g/l) and KCA (2.0 g/l) and uncharged solutes concentrations of 0.59 g/l and 2.42 g/l for glycerine and glucose, respectively. The rejections of the uncharged solutes, glucose

Table 5 Diffusion coefficients of the solutes at 15°C (Atkins 1994), Stokes radius ($r_{i,s}$) and cavity radius ($r_{i,cav}$)

	$D_i \times 10^{-9} \text{ (m}^2 \text{ s}^{-1}\text{)}$	$r_{i,s} \text{ (nm)}$	$r_{i,cav} \text{ (nm)}$
K^+	1.557	0.112	0.217 ²
Cl^-	1.621	0.108	0.194 ²
CA^-	0.625 ¹	0.265	0.283 ³
NH_4^+	1.562	0.112	0.213 ²
SO_4^{2-}	0.846	0.207	0.246 ⁴
H_2PO_4^-	0.702	0.250	0.268 ⁵
glucose	0.393	0.355	-
glycerol	0.718	0.258	-

1-Determined experimentally (Crow 1979, Atkins 1994)

2-Rashin and Honig 1985

3-The ionic radius was calculated based on the molar volume of clavulanic acid, assuming a spherical molecule

4-Based on the crystallographic radius of sulfate (Gemeay, *et al.* 2005)

5-Based on the crystallographic radius of PO_4^{3-} (Gemeay, *et al.* 2005)

and glycerol, are studied here as well, aiming to investigate the interactions between the uncharged solutes and the ions. This is not the complete composition of the real solution but a simplified one mimicking the complexity of the true industrial stream. This model solution was used to eliminate the variability of the real solution.

It was assumed that clavulanic acid is completely dissociated and, therefore, that it behaves like a monovalent ion. Furthermore, it was considered that the molecule has a spherical shape. The values of the radii and diffusivities of the ions considered in this work are shown in Table 5 as well as their source and the approximations needed to calculate these values.

3.4. Characterization of the membrane

The NF membrane was characterized in terms of structural and electrical parameters in order to obtain the parameters for the SEDE model.

3.4.1. Determination of the membrane structural characteristics

The two membrane structural characteristics depicted in Table 6 - effective average pore radius (r_p) and active layer thickness to porosity ratio ($\Delta x/A_k$), were obtained in a previous work by retention experiments of uncharged solutes (Cavaco Morão, *et al.* 2008).

3.4.2. Electrokinetic characterization of the membrane

The charge of the membrane was determined by tangential streaming potential (TSP) measurements for the six ions solution with the same composition as the solution used for the NF experiments. The effect on the membrane charge of the addition of uncharged solutes (glycerol and glucose) to the 6 ions mixture was also investigated.

TSP experiments were conducted with a ZETACAD zetameter (CAD Instrumentation) and the zeta potential was calculated using the extrapolation method (Fievet, *et al.* 2003, Sbaï, *et al.* 2003). The measurements were carried out through rectangular slit channels (length = 75 mm and width = 25 mm) of variable height, by using Teflon spacers of several thicknesses. The zeta potential was obtained from the intercept of the plot of $\Delta P/\Delta V$ versus the reciprocal channel height according the following equation (Yaroshchuk and Ribitsch 2002):

$$\left(\frac{\Delta P}{\Delta V}\right)_{I=0} = \frac{\mu\lambda_o}{\varepsilon_o\varepsilon_b\zeta} + \frac{2\mu h_m\lambda_m}{\varepsilon_o\varepsilon_b\zeta} \left(\frac{1}{h}\right) \quad (20)$$

The electrokinetic surface charge density, σ_{ek} , was estimated from zeta potential results through the Gouy-Chapman equation:

Table 6 Structural parameters of the membrane Desal DK

	Slit-like pores	Cylindrical pores
r_p (nm)	0.33	0.46
$\Delta x/A_k$ (μm)	3.89	2.76

$$\sigma_{ek} = -\text{sign}(\zeta) \sqrt{2\varepsilon_o\varepsilon_bRT \sum_i C_{i,f} \left(\exp\left(-\frac{z_i F \zeta}{RT}\right) - 1 \right)} \quad (21)$$

In order to apply the SEDE model, the volume charge density (X_{TSP}) was calculated assuming constant charge density, at a given bulk concentration, on the membrane surface and inside pores,

$$X_{TSP} = -\frac{\sigma_{ek}}{r_p F} \quad (\text{slit-like pores}) \quad (22)$$

or

$$X_{TSP} = -\frac{2\sigma_{ek}}{r_p F} \quad (\text{cylindrical pores}) \quad (23)$$

A simple correction was introduced by considering the dielectric constant of the solution inside pores, ε_p , instead of ε_b in Eq. (21) leading to (Szymczyk, *et al.* 2007):

$$X = X_{TSP} \sqrt{\frac{\varepsilon_p}{\varepsilon_b}} \quad (24)$$

It should be stressed that the application of the equations above is based on the arbitrary assumption that the zeta potential inside the pores is the same as that of the external membrane surface. Nevertheless, it is known that when two charged surfaces draw together, the surface charge density decreases and would tend to zero at contact, a phenomenon, known as “charge regulation” (Myers and Surfaces 1999). As the introduction of the charge regulation theory in the SEDE model is out of the scope of this work, the values of X determined from the TSP measurements can be considered as rough estimation of the true volume charge density.

3.5. Analytical methods

In order to calculate the observed rejections of the ions retentate and permeate concentrations were quantified using distinct analytical methods. Clavulanate concentration was determined using a spectrophotometric technique described in (Bird, *et al.* 1982). Ion chromatography was used to determine the anions concentration (Cavaco Morão, *et al.* 2008). Potassium was determined using a Jenway PFP7 flame photometer. The concentration of NH_4^+ was not determined experimentally but calculated so that the solutions electroneutrality was assured.

The concentration of glucose and glycerol were determined using an HPLC supplied by Waters (pump and controller model 600, autosampler model 717 Plus). The detection was performed using a refractive index (RI) detector Gilson 133 (Gilson Inc., USA). The column used was a PL Hi-Plex H (300×7.7 mm, 8 μm particle diameter) supplied by Polymer Laboratories. The eluent was H_2SO_4 0.01 M prepared with filtered (at 0.4 μm) deionised water. The flow rate was 0.6 ml/min and the temperature 70°C. The samples were injected in triplicate and the injection volume was 20 μl .

Conductivity was measured using a conductivity meter (Crison GLP31) and pH was measured by a pH meter (Crison Basic 20).

Table 7 Volume charge density inferred from TSP at pH 5.2 ± 0.2 assuming cylindrical and slit-like pores. Solutions: 1) 6 ions: $\text{KCl} + \text{KH}_2\text{PO}_4 + (\text{NH}_4)_2\text{SO}_4 + \text{KCA}$; 2) 6 ions and uncharged solutes (glucose and glycerol); 3) 10-fold concentrated solution with the 6 ions and uncharged solutes

Solutions:	$(X_{TSP} \text{ (mol m}^{-3}\text{)})$		
	6 ions	6 ions+uncharged solutes	6 ions+uncharged solutes 10-fold concentrated
I (mol m ⁻³)	25	25	250
Cylindrical pores:	-231	-231	-83
Slit-like pores:	-161	-161	-58

4. Results and discussion

4.1. Determination of the membrane charge density

The volume charge density (X_{TSP}) of the membrane contacting the distinct solutions, shown in Table 7, was computed by Eq. (22) or Eq. (23), assuming cylindrical and slit-like pores. The surface charge density (σ_{ek} , Eq. (21)), was calculated with the values of zeta potential obtained through the extrapolation method (Eq. (20)), *i.e.* TSP measurements at several channel heights. It should be noted that σ_{ek} is independent of the pore shape and the differences in the values of X_{TSP} for the two pore shapes results only from the geometrical factor applied to convert σ_{ek} into X_{TSP} (Eq. (22) or Eq. (23)). As illustrated in Table 7, considering the same solution, the magnitude of the X_{TSP} is larger if cylindrical pores are considered.

Even though the uncharged solutes do not contribute to the charging mechanisms there was, however, the possibility that they could influence the zeta potential through their adsorption onto the membrane surface and/or the variation of the properties of the solution (*e.g.* viscosity) and thus shifting the plane of shear. The influence of uncharged solutes on the zeta potential of the membrane was experimentally evaluated. From the results shown in Table 7 one can conclude that the volume charge density of the membrane contacting the six ions does not change with the addition of the uncharged solutes (glucose and glycerol).

The volume charge density of the membrane soaked in the 10-fold concentrated solution decreases relatively to the standard solution of six anions with uncharged solutes (*v.d.* Table 7). In fact, it can be hypothesized that the membrane volume charge in the 10-fold concentrated solution decreases due to both the screening of the proper charge of the membrane by counter-ions (counter-ions site-binding) and the competitive adsorption of co-ions and counter-ions on hydrophobic surface sites (Bandini 2005, Bruni and Bandini 2008). Nevertheless, this behaviour should not be emphasized because the concentration of the solution is too high ($I = 0.25 \text{ M}$), and at such high concentration, the streaming potential is too low to ensure accurate experimental measurements.

The experimental value of the volume charge of the 10-fold concentrated solution will be kept to use in the transport model, as this is still the best value available.

4.2. Rejection rates of multi-component solutions – experiments and model predictions

The NF application studied in this work is a concentration process and therefore, ideally, the rejection rates would be predicted as a function of concentration. In this work the model was applied just to predict the rejection rates in the initial feed solution and in the final concentrated

solution (10-fold concentrated solution). The modelling of the separation by NF of multi-component solutions was carried out for solutions of increasing complexity. It will be studied: 1) The separation of a multi-ionic solution comprising $(\text{NH}_4)_2\text{SO}_4$, KH_2PO_4 , KCl and KCA ; 2) The influence of the uncharged solutes (glucose and glycerol) in the separation of the ionic solutes and 3) The separation of the charged and uncharged solutes in a 10-fold concentrated solution.

4.2.1. Separation of ions and uncharged solutes

In this section the interactions between the uncharged solutes (glucose and glycerol) and the six ions (NH_4^+ , SO_4^{2-} , H_2PO_4^- , K^+ , Cl^- and CA^-) solution and their impact on the overall rejections will be investigated.

Influence of salts on the rejection rates of uncharged solutes

Fig. 2 shows the effect of the salts on the rejection rates of glucose and glycerol. The addition of salts contributed to raise the rejection of glycerol about 15% (in average). On the other hand, the rejection of glucose was not affected by the addition of salts to the solution. Glucose is almost totally retained by the membrane and therefore any variation towards the increase of its rejection rate can hardly be checked.

According to several authors (Bouchoux, *et al.* 2005, Bargeman, *et al.* 2005, Bouranene, *et al.* 2007) the rejection of an uncharged solute in the presence of salts is lower than that obtained with single solute solutions, which is in contradiction with our findings. These works were carried out with ion concentrations ranging from 0.1 to 1 M, *i.e.* at much higher concentrations than those currently used (total concentration of salts 0.016 M). Furthermore, it has also been reported that the uncharged solutes retention decreases with increasing salt concentration (Wang, *et al.* 2002, Bouchoux, *et al.* 2005, Bouranene, *et al.* 2007).

Several hypotheses have been postulated to explain this phenomenon (Bouchoux, *et al.* 2005, Bargeman, *et al.* 2005, Bouranene, *et al.* 2007). The first one is that the retention lowering is caused by an increase in the average pore size due to the repulsive interaction between the counter-ions

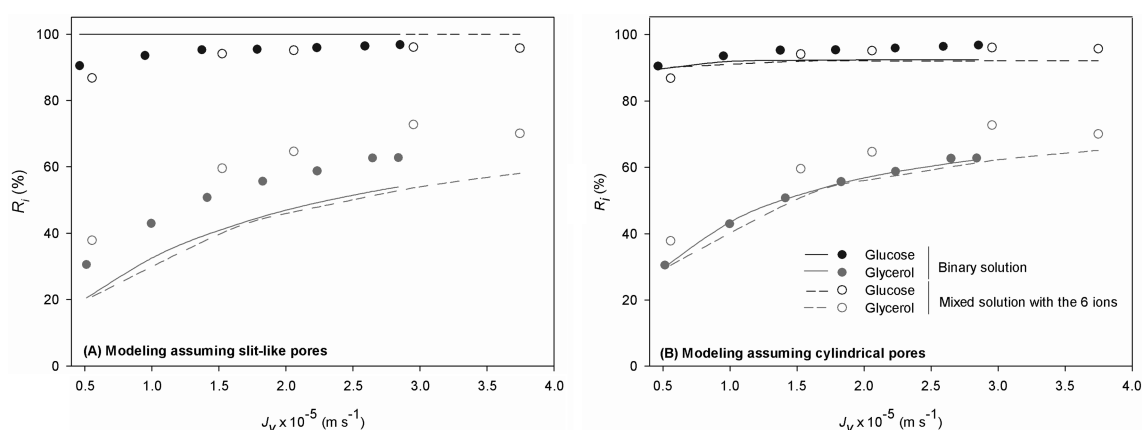


Fig. 2 Rejection of glucose and glycerol alone and in a mixed solution with the six ions. Comparison between the experimental rejections of glucose and glycerol (symbols) with the predictions of the uncharged solutes model (lines)

inside the pores. This phenomenon is usually referred as pore swelling. The second hypothesis is that the effective size of the neutral species is reduced: in the presence of ions the hydrated size of the uncharged solutes decreases because water preferentially solvate the ions. The decrease of the polyethyleneglycol (PEG) retention in the presence of ions by a NF ceramic membrane clarified that, in mixed solutions PEG/salts solutions, water preferentially solvates ions (Bouranene, *et al.* 2007). Consequently, the PEG molecules are partially dehydrated due to the presence of the surrounding ions.

In conclusion: in this work it is likely that the concentration of the added salts is too low either to evidence the effect of pore swelling and/or preferential hydration of the salts in detriment to the uncharged solutes.

Fig. 2 also shows the rejection rates of glucose and glycerol predicted by the hydrodynamic transport model - Eq. (17), both for the uncharged solutes alone and in the presence of the ions. The model was applied assuming slit-like pores or cylindrical pores with the membrane structural parameters depicted in Table 6. Clearly, the steric hindrance effects are better described assuming a cylindrical pore shape.

The addition of salts and glucose to the glycerol solution contributed also to increase the solution viscosity, which is meant to influence the retention of the solutes as well. The effect of increased viscosity was further investigated by performing calculations assuming that the viscosity of the solution is 1.01, 1.2, 1.5 and 2.0 - fold the viscosity of the bulk water. Based on the dependence of the viscosity with the concentration of glucose (Nabetani, *et al.* 1992), the increase of the bulk solution viscosity due glucose should be below 10%. Simulations were carried out also assuming higher increments of viscosity because it is expected that the salts as well as glycerol itself contribute to raise the viscosity.

The effect of the viscosity variation on the diffusivity of the solutes was corrected using the well known Stokes-Einstein. According to this equation, for each solute, i , the variation of viscosity and diffusivity are related by:

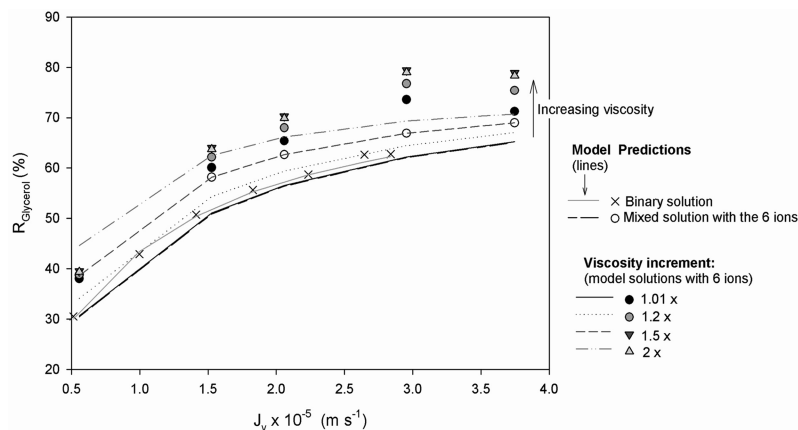


Fig. 3 Effect of viscosity increase (1.01, 1.2, 1.5, and 2 - fold the viscosity of the bulk water) on the rejection rate of glycerol in the mixed solution with the six ions and glucose. Comparison between the intrinsic rejection rates calculated from experimental data (symbols) and the predictions of the uncharged solutes model (lines). Note: the line for mixed solution with the 6 ions (—) and the line corresponding to a viscosity increase of 1.01x(—) are superposed

$$D_{i,2} = \frac{\mu_1}{\mu_2} D_{i,1} \quad (25)$$

The variation on the density of the solution was not considered. However, the increase of the solution viscosity leads to a higher concentration polarization and, as a consequence, the intrinsic rejection rates of glycerol calculated with the experimental data of $C_{i,p}$ grow. As it can be observed in Fig. 3 the agreement between the intrinsic rejection rates calculated from the experimental values of $C_{i,p}$ and the model predictions did not improve significantly.

Influence of uncharged solutes on the rejection rates of salts

The TSP measurements showed that the presence of glucose and glycerol did not modify significantly the membrane surface charge (*v.d.* Table 7). As shown in previous publications (Cavaco Morão, *et al.* 2008, 2008a) the rejection rates of the 5 or 6 ions are well described considering that steric, electric (Donnan) and Born dielectric exclusion mechanisms govern membrane selectivity. Fig. 4 shows that the best fitting of the model to the experimental data is obtained if ϵ_p is raised from 59 to 62 for the solution with uncharged solutes (assuming slit-like pores). Nonetheless, the fitted model suggests a slight decrease in the Cl^- rejection, in the presence of uncharged solutes. Within the experimental error in the determination of the rejection rates the physical meaning of this difference is doubtful. In this case, if a cylindrical pore shape is assumed, the suitability of the model to describe the experimental data is not altered (*v.d.* Table 8). A similar

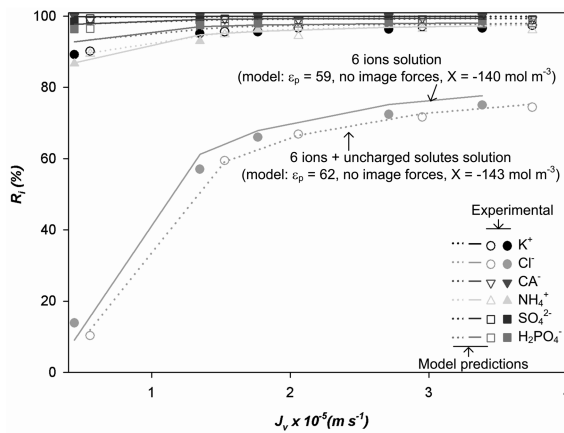


Fig. 4 Rejection rates of the six ions and in mixed solutions with glucose and glycerol. Model predictions (SEDE without “image forces”) assuming slit-like pores and fitting ϵ_p . Closed symbols and solid lines: 6 ions solution. Open symbols and dashed lines: 6 ions solution+glycerol+glucose. Note: The rejection rates predicted by the model for K^+ and NH_4^+ are superposed; the “experimental” intrinsic rejection rates of CA^- and SO_4^{2-} are roughly coincident

Table 8 Comparison of the fit (values of S_p) for slit-like and cylindrical pores geometries, neglecting image forces

	Slit-like pores	Cylindrical pores
6 ions solution	0.018	0.017 ($X = -224 \text{ mol m}^{-3}$, $\epsilon_p = 74$)
6 ions solution+uncharged solutes	0.010	0.009 ($X = -231 \text{ mol m}^{-3}$, $\epsilon_p = 78$)

fitting of the model is obtained with $\varepsilon_p = 74$ and 77 , respectively for the electrolyte solution and for the solution of ions and uncharged solutes (results not shown). As previously observed the role of the Born dielectric exclusion in the separation of the ions diminishes if it is assumed that the pores have a cylindrical shape. In Table 8 a comparison is made between the results obtained for the two pore geometries.

The decrease of the salt rejection in the presence of a neutral solute has been reported by other authors (Szaniawska and Spencer 1997, Bouchoux, *et al.* 2005). The explanations that have been suggested are related to the increase of concentration polarization due to the higher viscosity near the membrane surface. The latter can be caused by the presence of the neutral solute. However, according to Bouchoux, *et al.* (2005) this difference is not always clear and depends on the membrane. As a conclusion we can observe that for the prevailing conditions the interaction between the charged and uncharged solutes in this mixture is not very significant.

4.2.2. Separation of ions and uncharged solutes - concentrated solution

In this section, the separation of the charged and uncharged solutes was investigated using a solution 10-fold concentrated. Fig. 5 presents the intrinsic rejection rates of the ions, calculated from the observed rejection rates as well as the model predictions, assuming steric, electric and Born dielectric exclusion (assuming cylindrical and slit-like pores). First of all, it should be pointed out that the rejections of the concentrated solution are much lower (compare with Fig. 4). The decrease in the rejection rates with increasing salt concentration is a consequence of the electric exclusion mechanism (*e.g.* Cavaco Morão, *et al.* 2006). This effect is particularly evident for chloride (small monovalent ion) which shows negative rejections. Contrasting with the results obtained with the more dilute solutions, as it can be observed in Fig. 5, the SEDE model (neglecting the “image forces” and fitting ε_p) shows several shortcomings to describe the separation of the ions in the concentrated solution. The most obvious problems noticed are:

- The shape of the curve for Cl^- rejection is not well predicted;
- Both H_2PO_4^- and CA^- rejections are underestimated;

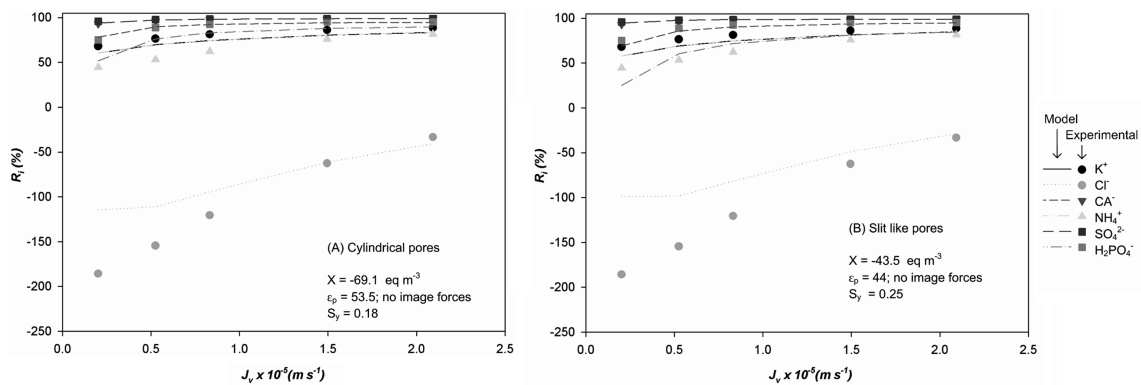


Fig. 5 Comparison between the SEDE predictions and intrinsic rejection rates based on the experimental data of each ion in solution. “Image forces” were neglected and ε_p was fitted. Pores were modeled as: (A) cylinders and (B) slits. Note: The rejection rates predicted by the model for K^+ and NH_4^+ are superposed; the “experimental” intrinsic rejection rates of CA^- and SO_4^{2-} are roughly coincident

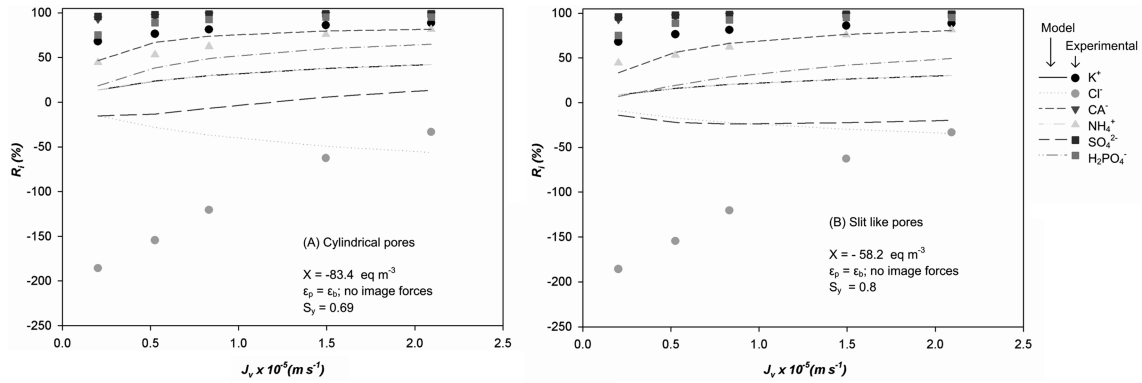


Fig. 6 Comparison between the model predictions and the intrinsic rejection rates based on the experimental data of each ion in the concentrated solution. Only steric and electric exclusion mechanisms were considered and pores were modeled as (A) cylinders and (B) slits. Note: The rejection rates predicted by the model for K^+ and NH_4^+ are superposed; the “experimental” intrinsic rejection rates of CA^- and SO_4^{2-} are roughly coincident

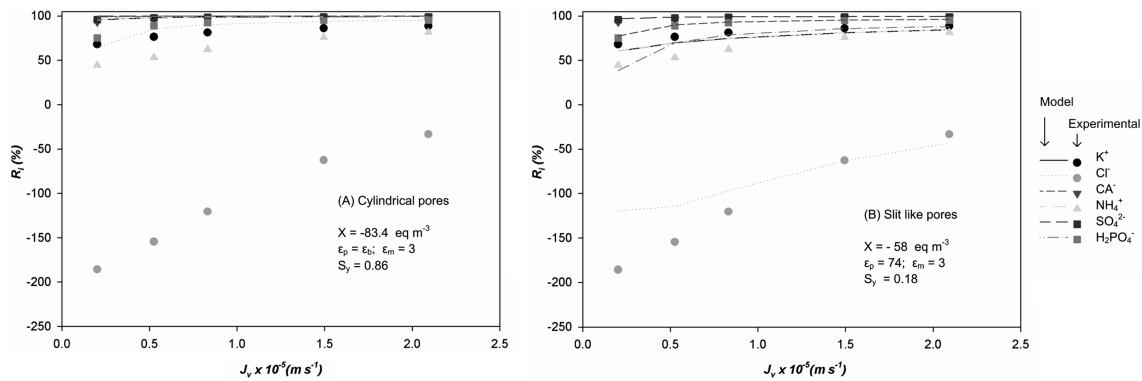


Fig. 7 Comparison between the SEDE model predictions and the intrinsic rejection rates based on the experimental data of each ion in the concentrated solution. Pores were modeled as (A) cylinders and (B) slits. Notes: the “experimental” intrinsic rejection rates of CA^- and SO_4^{2-} are roughly coincident; (A) the predictions for K^+ and NH_4^+ and for SO_4^{2-} , $H_2PO_4^-$ and CA^- are superposed; (B) the rejection rates predicted by the model for K^+ and NH_4^+ are superposed

- Considering the rejection rates based on the experimental data the following order is observed: $R_{H_2PO_4^-} > R_{K^+}$. Regardless the pore shape assumed in the model, the predicted rejection order of these ions is inversed at low permeation fluxes.

- The rejection rates of K^+ and NH_4^+ determined from experiments are different ($R_{K^+} > R_{NH_4^+}$) while the model predictions are coincident.

It was verified, for both pores geometry, that the model description of the experimental data was not improved, neither considering only electric and steric exclusion (Fig. 6), nor even considering all the exclusion effects, as shown in Fig. 7.

For the case considered in Fig. 7 (B), the value of S_y being not so high is, however, one order of magnitude higher than the same value for the diluted solution (see Table 8). As expected, the model

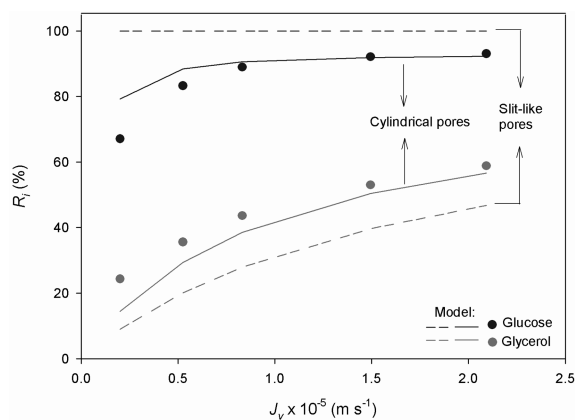


Fig. 8 Rejection of glucose and glycerol a mixed with the six ions – 10-fold concentrated solution. Comparison between the experimental rejections of glucose and glycerol (symbols) with the predictions of the uncharged solutes model (lines)

accounting only for steric and electric exclusion fails completely to describe rejection rates of this ions solution. Likewise for the solutions studied in the previous sections, the inclusion of the “images forces” dielectric exclusion did not enhance the model. Thus, the modeling of the rejection rates of this concentrated solution should be made considering only steric, electric and Born dielectric exclusion (ϵ_p fitted), as shown in Fig. 5.

The shortcomings of the model to describe the rejection rates of the ions in the concentrated solution are likely to be related with the higher ionic strength. The following explanations are hypothesized:

- (1) The deviations to ideality are more significant and the activity coefficients must be included;
- (2) As the ionic strength can influence electrostatic interaction between the membrane functional groups, the membrane cross-linked polymer network can either expand or shrink in response to variations in solution ionic strength. Consequently, this may induce changes in the membrane pore size and thus influence retention characteristics;
- (3) Electrostatic interaction between the ions leading to the aggregation of solutes, resulting in the increase of the effective solutes radii and/or decrease of the diffusion coefficient. The decrease of the diffusion coefficient can result also from the solutes-solutes interactions which are expected to be more significant at higher concentrations.

Finally, in Fig. 8 the rejection rates of the uncharged solutes in the concentrated solution are shown. Considering cylindrical pores, the rejection rates of glucose and glycerol are well described by the size exclusion model (Eq. (17)). On the contrary, in Fig. 2 (lower concentration solution) it was observed that the rejection of glycerol, in the mixed solution with salts, was higher than the model predictions. According to Fig. 8, increasing the solution concentration vanishes this effect. It is likely that, in the case of the concentrated solution, due to the increased salt concentration (0.16 M), the effective size of the uncharged species decreases more significantly. As previously mentioned, water preferentially solvates the ions and, at high salt concentrations, the effective size of uncharged species decreases (Bouranene, *et al.* 2007). Therefore, the rejection of glycerol is expected to decrease as well.

5. Conclusions

The conceptual simplicity of the SEDE model makes it a useful starting point for the investigation of the retention of individual ions in multi-ionic solutions. It has been shown that the predicted intrinsic rejections, at moderate concentrations, for the multi-component solution studied are quite satisfactory considering the shortcomings of the transport model, the complexity of the solution and that only a single parameter, ε_p , was fitted. For the 10-fold concentrated solution, however, the match between the model predictions and the rejection rates based on the NF experiments is rather poor.

It was found that the interaction between the charged and uncharged solutes in the six ions mixture is not very significant. The striking effect observed was the increase (relative deviations between 8 and 24%) of the glycerol rejection in the presence of the salts and glucose.

Acknowledgments

The PhD grant SFRH/BD/18496/2004 is gratefully acknowledged by Cavaco Morão, A.I. We wish also to thank to CIPAN S.A for supplying the potassium clavulanate and for their assistance in the realization of the NF experiments.

References

- Atkins, P.W. (1994), *Physical chemistry*, 6th edition, University Press, Oxford.
- Bandini, S. and Vezzani, D. (2003), "Nanofiltration modeling: the role of dielectric exclusion in membrane characterization", *Chem. Eng. Sci.*, **58**, 75-86.
- Bandini, S. (2005), "Modelling the mechanism of charge formation in NF membranes: Theory and application", *J. Membrane Sci.*, **264** (2005), 75-86.
- Bargeman, G., Vollenbroek, J.M., Straatsma, J., Schröen, C.G.P.H. and Boom, R.M. (2005), "Nanofiltration of multicomponent feeds. Interactions between neutral and charged components and their effect on retention", *J. Membrane Sci.*, **247**, 11-20.
- Bird, A.E., Bellis, J.M. and Gasson, B.C. (1982), "Spectrophotometric assay of clavulanic acid by reaction with imidazole", *Analyst*, **107**, 1241-1245.
- Bouchoux, A., Roux-de Balmann, H. and Lutin, F. (2005), "Nanofiltration of glucose and sodium lactate solutions. Variations of retention between single and mixed solute solutions", *J. Membrane Sci.*, **258**, 123-132.
- Bouranene, S., Szymczyk, S., Fievet, P. and Vidonne, A. (2007), "Influence of inorganic electrolytes on the retention of polyethyleneglycol by a nanofiltration ceramic membrane", *J. Membrane Sci.*, **290**, 216-221.
- Bowen, W.R. and Welfoot, J.S., (2002), "Modelling of membrane nanofiltration - pore size distribution effects", *Chem. Eng. Sci.*, **57**, 1393-1407.
- Bowen, W.R. and Mukhtar, H., (1996), "Characterisation and prediction of separation performance of nanofiltration membranes", *J. Membrane Sci.*, **112**, 263-274.
- Bruni, L. and Bandini, S. (2008), "The role of the electrolyte on the mechanism of charge formation in polyamide nanofiltration membranes", *J. Membrane Sci.*, **308**, 136-151.
- Capelle, N., Moulin, P., Charbit, F. and Gallo, R. (2002), "Purification of heterocyclic drug derivatives from concentrated saline solution by nanofiltration", *J. Membrane Sci.*, **196**, 125-141.
- Cavaco Morão, A.I., Brites Alves, A.M. and Afonso, M.D. (2006), "Concentration of clavulanic acid broths: influence of surface charge density on NF performance", *J. Membrane Sci.*, **281**, 417-428.
- Cavaco Morão, A.I., Szymczyk, A., Fievet, P. and Brites Alves, A.M. (2008), "Modelling the separation by nanofiltration of a multi-ionic solution relevant to an industrial process", *J. Membrane Sci.*, **322**, 320-330.
- Cavaco Morão, A.I., Szymczyk, A., Fievet, P. and Brites Alves, A.M. (2008a), "Modelling the separation by

- nanofiltration for a multi-ionic solution: application to an industrial process”, *Proc. of Engineering with Membranes 2008*, pp. 287, Algarve, Portugal, May 25-28.
- Cavaco Morão, A.I., Brites Alves, A.M. and Geraldes, V. (2008b), “Concentration polarization in a reverse osmosis/nanofiltration plate-and-frame membrane module”, *J. Membrane Sci.*, **325**, 580-591.
- Dechadilok, P. and Deen, W.M. (2006), “Hindrance factors for diffusion and convection in pores”, *Ind. Eng. Chem. Res.*, **45**, 6953-6959.
- Deen, W.M. (1987), “Hindered transport of large molecules in liquid-filled pores”, *AICHE J.* **33**, 1409-1425.
- Fievet, P., Sbaï, M., Szymczyk, A. and Vidonne, A. (2003), “Determining the ζ - potential of plane membranes from tangential streaming measurements: effect of the membrane body conductance”, *J. Membrane Sci.*, **226**, 227-236.
- Gemeay, A.H., Mansour, I.A., El-Sharkawy, R.G. and Zaki, A.B. (2005), “Preparation and characterization of pylaniline/manganese dioxide composites via oxidative polymerization: effect of acids”, *Eur. Polym. J.*, **41**, 2575-2583.
- Geraldes, V. and Afonso, M.D. (2007), “Prediction of the concentration polarization in the nanofiltration/reverse osmosis of dilute multi-ionic solutions”, *J. Membrane Sci.*, **300**, 20-27.
- Myers, D. and Surfaces, I. (1999), *Interfaces and colloids - principles and applications*, 2nd edition, John Wiley and Sons, New York.
- Nabetani, H., Nakajima, M. and Watanabe, A. (1992), “Nakao S., Kimura, S., Prediction of the flux for the reverse osmosis of a solution containing sucrose and glucose”, *J. Chem. Eng. Jap.*, **25**, 575-580.
- Rashin, A.A. and Honig, B. (1985), “Reevaluation of the Born model of ionic hydration”, *J. Phys. Chem.*, **89**, 5588-5593
- Sbaï, M., Szymczyk, A., Fievet, P., Sorin, A., Vidonne, A., Pellet-Rostaing, S., Favre-Reguillon, A. and Lemaire, M. (2003), “Influence of the membrane pore conductance on tangential streaming potential”, *Langmuir*, **19**, 8867-8871.
- Shäfer, A.I., Fane, A.G. and Waite, T.D. (2005), *Nanofiltration - Principles and Applications*, Elsevier, Oxford.
- Szaniawska, D. and Spencer, H.G. (1997), “Non-equilibrium thermodynamics analysis of the transport properties of formed-in-place Zr(IV) hydrous oxide-polyacrylate membranes: III. Ternary lactose-NaCl-water solutions”, *Desalination*, **113**, 1-6.
- Szymczyk, A. and Fievet, P. (2005), “Investigating transport properties of nanofiltration membranes by means of a steric, electric and dielectric exclusion model”, *J. Membrane Sci.*, **252**, 77-88.
- Szymczyk, A., Fatin-Rouge, N., Fievet, P., Ramseyer, C. and Vidonne, A. (2007), “Identification of dielectric effects in nanofiltration of metallic salts”, *J. Membrane Sci.*, **287**, 102-110.
- Szymczyk, A., Fatin-Rouge, N. and Fievet, P. (2007b), “Tangential streaming potential as a tool in modeling of ion transport through nanoporous membranes”, *J. Colloid Interf. Sci.*, **309**, 245-252.
- Szymczyk, A., Sbaï, M., Fievet, P. and Vidonne, A. (2006), “Transport properties and electrokinetic characterization of an amphoteric nanofilter”, *Langmuir*, **22**, 3910-3919.
- Van der Bruggen, B., Mänttari, M. and Nyström, M. (2008), “Drawbacks of applying nanofiltration and how to avoid them: A review”, *Sep. Purf. Techn.*, **66**, 251- 263.
- Wang, X.L., Zhang, C. and Ouyang, P. (2002), “The possibility of separating saccharides from a NaCl solution by using nanofiltration in diafiltration mode”, *J. Membrane Sci.*, **204**, 271-281.
- Yaroshchuk, A.E. (2000), “Dielectric exclusion of ions from membranes”, *Adv. Colloid Interf. Sci.*, **85**, 193-230.
- Yaroshchuk, A.E. and Ribitsch, V. (2002), “Role of channel wall conductance in the determination of ζ - potential from electrokinetic measurements”, *Langmuir*, **18**, 2036-2038.

List of symbols

A_k	porosity of the membrane active layer
C	molar concentration of the solution (mol m^{-3})
C_i	molar concentration of solute i in the solution (mol m^{-3})
$C_{i,f}$	molar concentration of solute i in the feed solution (mol m^{-3})

$C_{i,m}$	molar concentration of solute i at the membrane surface (mol m^{-3})
$C_{i,p}$	molar concentration of solute i in the permeate (mol m^{-3})
D_i	diffusivity of solute i at infinite dilution ($\text{m}^2 \text{s}^{-1}$)
e	electron charge (C)
F	Faraday constant, 96486.7 (C eq ⁻¹)
h	channel height (m)
h_m	effective thickness in which the conduction current flows inside the porous. body of the membrane (m)
I	ionic strength (mol m^{-3})
j_i	molar flux density of ion i ($\text{mol s}^{-1} \text{m}^2$)
J_v	permeation flux ($\text{mol s}^{-1} \text{m}^2$)
k	Boltzmann constant ($1.38 \times 10^{-23} \text{ J K}^{-1}$)
k_i	mass transfer coefficient for solute i (m s^{-1})
k_i^*	mass transfer coefficient for solute i dependent on the permeation flux (m s^{-1})
$K_{i,c}$	hydrodynamic coefficient accounting for the effect of pore walls on convective transport.
$K_{i,d}$	hydrodynamic coefficient for hindered transport inside pores
N_A	Avogadro number ($6.22 \times 10^{23} \text{ mol}^{-1}$)
P	pressure (Pa)
Pe	Peclet permeation number
R	gas constant, 8.314 ($\text{J mol}^{-1} \text{K}^{-1}$)
Re	Reynolds number, $Re = \rho v_o h / \mu$
R_i	intrinsic rejection rate of solute i , $R_i = 1 - C_{i,p} / C_{i,m}$
$R_{i,obs}$	observed rejection rate of solute i , $R_{i,obs} = 1 - C_{i,p} / C_{i,f}$
$r_{i,cav}$	cavity radius of ion i (m)
$r_{i,s}$	stokes radius of ion i (m)
r_p	pore radius (m)
Sc_i	Schmidt number, $Sc_i = \mu / \rho D_i$
Sh_i	Sherwood number, $Sh_i = k_i h / D_i$
S_y	least squares objective function (v.d. Eq. 19)
T	absolute temperature (K)
v_o	cross flow velocity in the feed channel (m s^{-1})
V	fluid velocity inside pores (m s^{-1})
X	membrane volume charge density (mol m^{-3})
X_{TSP}	membrane volume charge density derived from TSP (mol m^{-3})
z_i	charge number of ion i

Greek symbols

$\Delta x / A_k$	membrane active layer thickness to porosity ratio (m)
$\Delta \psi$	Donnan potential involved in the electric exclusion mechanism (V)
ρ	density (kg m^{-3})
μ	dynamic viscosity in free solution (Pa. s)
ζ	zeta potential (V)
λ_0	solution conductivity (S m^{-1})
ϵ_0	vacuum permittivity, $8.8542 \times 10^{-12} \text{ C}^2 \text{ J}^{-1} \text{ m}^{-1}$
ϵ_b	dielectric constant of the bulk solution, 78.54 at 25°C

σ_{ek}	electrokinetic charge density ($C\ m^{-2}$)
Φ_i	equilibrium partition coefficient for steric interactions
λ_i	ratio of solute radius to pore radius, $\lambda_i = r_{i,s}/r_p$
λ_m	conductivity inside the porous body of the membrane ($S\ m^{-1}$)
ε_m	dielectric constant of the membrane
ε_p	dielectric constant of the solution inside pores
$\Delta W_{i,Born}$	excess solvation energy due to Born effect for ion i (J)
$\Delta W_{i,im}$	solvation energy due to “image forces” for ion i (J)
ΔP	pressure difference (P)
ΔV	streaming potential (V)
γ_i	activity coefficient of ion i in solution ($mol\ m^{-3}$)
κ^{-1}	Debye length (m)
ξ	electrical potential gradient at the feed solution/ membrane interface (V)
Ξ	mass transfer coefficient correction factor, $\Xi = \frac{k_i^*}{k_i}$
Ψ	local electrical potential inside the pores (V)